Dynamical structure factor of one-dimensional hard rods

M. Motta,[1] E. Vitali,[1] M. Rossi,[2,3] D. E. Galli,[4] and G. Bertaina[4]
[1]*Department of Physics, College of William and Mary, Williamsburg, Virginia 23187-8795, USA*
[2]*Scuola Normale Superiore, Piazza dei Cavalieri 7, I-56126 Pisa, Italy*
[3]*International Center for Theoretical Physics (ICTP), Strada Costiera 11, I-34154 Trieste, Italy*
[4]*Dipartimento di Fisica, Università degli Studi di Milano, via Celoria 16, I-20133 Milano, Italy*
(Received 27 August 2016; published 13 October 2016)

The zero-temperature dynamical structure factor $S(q,\omega)$ of one-dimensional hard rods is computed using state-of-the-art quantum Monte Carlo and analytic continuation techniques, complemented by a Bethe ansatz analysis. As the density increases, $S(q,\omega)$ reveals a crossover from the Tonks-Girardeau gas to a quasisolid regime, along which the low-energy properties are found in agreement with the nonlinear Luttinger liquid theory. Our quantitative estimate of $S(q,\omega)$ extends beyond the low-energy limit and confirms a theoretical prediction regarding the behavior of $S(q,\omega)$ at specific wave vectors $\mathcal{Q}_n = n2\pi/a$, where a is the core radius, resulting from the interplay of the particle-hole boundaries of suitably rescaled ideal Fermi gases. We observe significant similarities between hard rods and one-dimensional ^{4}He at high density, suggesting that the hard-rods model may provide an accurate description of dense one-dimensional liquids of quantum particles interacting through a strongly repulsive, finite-range potential.

DOI: 10.1103/PhysRevA.94.043627

I. INTRODUCTION

One-dimensional (1D) quantum systems are subject to intense research, due to their theoretical and experimental peculiarities [1–3]. On the theoretical side, the reduced dimensionality enhances quantum fluctuations and interaction, giving rise to unique phenomena such as the nonexistence of Bose-Einstein condensation [4–8] and the breakdown of Fermi-liquid behavior [9]. On the experimental side, a 1D system is realized when a three-dimensional (3D) system is loaded into an elongated optical trap or confined into a narrow channel, and the transverse motion is frozen to zero-point fluctuations.

Remarkably, several 1D many-body models of considerable conceptual and experimental relevance are exactly solvable [10–15] and provide a precious support for understanding static and dynamic properties of interacting 1D systems in suitable regimes [16–28]. In particular, the behavior of 1D systems with a hard-core repulsive interaction, like ^{4}He or other gases adsorbed in carbon nanotubes [28–32], can be understood by making the assumption that particles behave like a gas of impenetrable segments or hard rods (HRs). Indeed, at high density, the principal effect of a short-range hard-core repulsive interaction is volume exclusion. Therefore, a reasonable approximation of the actual microscale behavior of the system can be obtained by taking into account the volume exclusion phenomenon only, neglecting all other details of the interaction; within this approach, the system is described as an assembly of HRs of a suitable length a.

The recognition that volume exclusion is the most important factor in analyzing short-range hard-core repulsive interactions in high-density classical systems dates back to the seminal work by van der Waals [33] and Jeans [34]. It was later recognized [35,36] that the statistical mechanics of a system of classical HRs is exactly solvable. In 1940 Nagamiya proved [10] that also a system of quantum HRs is exactly solvable using the Bethe ansatz technique and imposing a special system of boundary conditions. Nagamiya's treatment was later adapted by Sutherland [14] to the more familiar periodic boundary conditions.

It is remarkable that local properties of the HR model are independent of the particles being bosons or fermions [7], since in 1D the hard-core interaction creates nodes in bosonic wave functions which can be completely mapped to the nodes of fermionic wave functions. Only nonlocal properties differ, such as the momentum distribution [31].

Even if the eigenfunctions and eigenvalues of the HR model can be determined exactly, so far the only systematic way to obtain a complete description of the ground-state correlation functions of the model has been the variational Monte Carlo (VMC) method [31,32]. Dynamical properties have also been addressed by using the variational Jastrow-Feenberg theory in [37].

In the present work, we resort to state-of-the-art projective quantum Monte Carlo (QMC) [38–40] and analytic continuation [41] techniques to compute the dynamical structure factor, $S(q,\omega)$, of a single-component system of HRs. This analysis is supported by the Bethe ansatz solution of the elementary excitations of the model, following [12].

The dynamical structure factor characterizes the linear response of the system to an external field which weakly couples to the density. In the context of quantum liquids, it can be probed via inelastic neutron scattering [42,43], while in the ultracold gases field it can be probed with Bragg scattering [27,44], also implemented via digital micromirror devices [45] or cavity-enhanced spontaneous emission [46].

While the low-energy properties of $S(q,\omega)$ are universal and can be described by the Tomonaga-Luttinger liquid (TLL) theory [47–51] and its recent and remarkable generalization, called the nonlinear TLL theory [3,52], high-energy properties depend explicitly on the shape of the interaction potential and lie in a regime beyond the reach of those theoretical approaches. Due to such limitations, we rely on QMC to estimate $S(q,\omega)$ for all momenta and energies.

The HR model, and its solution by Bethe ansatz, is described in Sec. II. The methods used to compute the dynamical structure factor are reviewed in Sec. III. Results are presented and discussed in Sec. IV, and conclusions are drawn in the last section, Sec. V.

II. THE HARD-RODS MODEL

Hard rods are the 1D counterpart of 3D hard spheres [31,32]. The interparticle hard-rod potential is

$$V_{HR}(r) = \begin{cases} \infty & |r| \leqslant a \\ 0 & |r| > a \end{cases}, \tag{1}$$

where a is the rod size. The Hamiltonian of a system of N particles inside an interval $[0,L]$ of length L with interparticle HR potential is

$$H = -\frac{\hbar^2}{2m}\sum_{i=1}^{N}\frac{\partial^2}{\partial r_i^2} + \sum_{i<j=1}^{N} V_{HR}(r_i - r_j), \tag{2}$$

where m is the mass of the particles and $(r_1 \dots r_N) \in \mathbb{R}^N$ their coordinates. The domain of the Hamiltonian operator (2) is the set of wave functions $\Psi(r_1 \dots r_N) \in \mathcal{L}^2(\mathbb{R}^N)$ such that

$$\begin{aligned} &\Psi(r_1 \dots r_i \dots r_j \dots r_N) = \pm\Psi(r_1 \dots r_j \dots r_i \dots r_N), \\ &\Psi(r_1 \dots r_i + L \dots r_N) = \Psi(r_1 \dots r_i \dots r_N), \\ &\Psi(r_1 \dots r_i \dots r_j \dots r_N) = 0 \quad \text{if } |r_i - r_j| \leqslant a, \end{aligned} \tag{3}$$

for any $i \neq j$. The first of the conditions (3) imposes Bose or Fermi symmetry, the second imposes periodic boundary conditions (PBCs), and the third guarantees that $\langle\Psi|H|\Psi\rangle < \infty$. Thanks to the second equation in (3), we can concentrate on positions $(r_1 \dots r_N) \in \mathcal{C} = [0,L]^N$.

A. Solution by Bethe ansatz

The solution of the HR Hamiltonian (2) was first addressed by Nagamiya [10], relying on the Bethe ansatz method [53]. The author substituted PBC (3) with slightly different boundary conditions, motivated by the study of particles arranged on a circle [10]. The solution of the HR Hamiltonian by Bethe ansatz was subsequently addressed by Sutherland in [14], applying PBC.

In the present section, we provide a detailed review of the solution of the HR model following the method of Refs. [11] and [12], and a detailed description of its elementary excitations. This is a key ingredient that permits us to characterize the singularities of $S(q,\omega)$ predicted by the nonlinear Luttinger liquid theory (Sec. II D).

In order to solve the HR Hamiltonian (2), following Ref. [10], let us concentrate on the sector $\mathcal{S}$ of the configuration space $\mathcal{C}$ where

$$\begin{aligned} &0 < r_1 < r_2 - a \\ &r_{i-1} + a < r_i < r_{i+1} - a \quad i = 2 \dots N-1 \\ &r_{N-1} + a < 7r_N < L - a, \end{aligned} \tag{4}$$

which is related to all other sectors of the configuration space by a combination of permutations and translations of the particles, and eliminate the rod size a by the transformation

$$x_i = r_i - (i-1)a. \tag{5}$$

The rod coordinates x_i lie in the set

$$0 < x_1 < x_2 < \cdots < x_N < L', \tag{6}$$

where $L' = L - Na$ is called the unexcluded volume. The HR Hamiltonian (2) then takes the form

$$H = -\frac{\hbar^2}{2m}\sum_{i=1}^{N}\frac{\partial^2}{\partial x_i^2}, \tag{7}$$

and the third condition (3), imposing that particles collide with each other as impenetrable elastic rods, can be correspondingly expressed as

$$\tilde{\Psi}(x_1 \dots x_i \dots x_j \dots x_N) = 0 \quad \text{if } x_i = x_j, \tag{8}$$

where we introduce the notation

$$\Psi(r_1\, r_2 \dots r_N) = \tilde{\Psi}(x_1, \dots x_N), \quad (r_1\, r_2 \dots r_N) \in \mathcal{S} \tag{9}$$

to express Ψ in terms of the rod coordinates. Eigenfunctions of (7) satisfying the condition (8) have the form [10]

$$\tilde{\Psi}(x_1 \dots x_N) = \frac{1}{\sqrt{N!}}\det\left(\frac{e^{ik_i x_j}}{\sqrt{L'}}\right), \tag{10}$$

where $k_1 \dots k_N$ are a set of quantum numbers called quasi-wave vectors, that will be identified later. The energy eigenvalue corresponding to (10) is $E_{\{k\}} = \frac{\hbar^2}{2m}\sum_{i=1}^{N} k_i^2$. Moreover, (10) is identically zero if and only if any two quasi-wave vectors coincide. The values of the quasi-wave vectors $k_1 \dots k_N$ are fixed imposing PBC to the wave functions (10). Practically, imposing PBC means requiring that

$$\Psi(0\, r_2 \dots r_N) = \Psi(L\, r_2 \dots r_N) \tag{11}$$

for all $r_2 \dots r_N$. Merging (10) and (11), one finds that PBC are satisfied if, for all quasi-wave vectors k_i, the following condition holds [14]:

$$(k_i - K)\,a = k_i[L - (N-1)a] - 2\pi n_i + \xi^{B,F}(N), \tag{12}$$

where $i = 1 \dots N, K = \sum_{i=1}^{N} k_i, n_i \in \mathbb{Z}$ is an integer number, $\xi^F(N) = 0$, and

$$\xi^B(N) = \begin{cases} 0 & \text{for } N \text{ odd} \\ \pi & \text{for } N \text{ even} \end{cases}. \tag{13}$$

Equation (12) leads easily to

$$k_i = \frac{2\pi}{L'}n_i - \frac{1}{L'}\xi^{B,F}(N) - \frac{aK}{L'}. \tag{14}$$

Remarkably, even if the quasi-wave vectors k_i are constructed with both L and L', the total momentum K is an integer multiple

$$K = \frac{2\pi}{L}\sum_{i=1}^{N} n_i - \frac{N\xi^{B,F}(N)}{L} \tag{15}$$

of $\frac{2\pi}{L}$. To summarize, the eigenfunctions of the HR Hamiltonian are in one-to-one correspondence with combinations of N integer numbers without repetition.

B. Ground-state properties

For a system of N Bose hard rods, the ground-state wave function is characterized by quasi-wave vectors

$$k_{i,GS} = \frac{2\pi}{L'} n_{i,GS}, \qquad n_{i,GS} = -n_F + (i-1), \tag{16}$$

symmetrically distributed around 0, with $n_F = (N-1)/2$. The ground-state wave vector is naturally $K = 0$. The ground-state energy reads [10,31]

$$E_{GS} = \frac{\hbar^2}{2m}\left(\frac{2\pi}{L'}\right)^2 \frac{n_F(n_F+1)(2n_F+1)}{3}. \tag{17}$$

In the thermodynamic limit of large system size N at constant linear density $\rho = N/L$, the ground-state energy per particle converges to

$$E_\infty = \lim_{N\to\infty} \frac{E_{GS}}{N} = \frac{\hbar^2 k_F^2}{6m(1-\rho a)^2}, \tag{18}$$

where $k_F = \pi\rho$ is defined in analogy with the fermionic case. The reduced dimensionality is responsible for the *fermionization* of impenetrable Bose particles: the strong repulsion between particles mimics the Pauli exclusion principle [7]. In particular, the limit $\rho a = 0$ corresponds to the well-known Tonks-Girardeau gas, namely, the hard-core limit of the Lieb-Liniger model [11], where all local properties are the same as for the ideal Fermi gas (IFG). At finite ρa, we can think of HRs as evolving from the Tonks-Girardeau gas, in that the infinitely strong repulsive interaction is accompanied by an increasing volume exclusion. HRs are therefore a model for the *super* Tonks-Girardeau gas, which has been predicted and observed [18,54–57] as a highly excited and little compressible state of the attractive Lieb-Liniger Bose gas, in which no bound states are present.

In the case of hard rods, the eigenfunctions of both Bose and Fermi systems have the same functional form in the sector $\mathcal{S}$ of the configuration space; away from $\mathcal{S}$, they differ from each other only by a sign associated to a permutation of the particles [7]. Therefore, the matrix elements of local operators like the density fluctuation operator

$$\rho_q = \sum_{i=1}^{N} e^{-iqr_i} \tag{19}$$

are identical for Bose and Fermi particles. This, in particular, implies that the dynamical structure factor

$$S(q,\omega) = \int_{-\infty}^{\infty} dt\, \frac{e^{i\omega t}}{2\pi N} \langle\Psi| e^{itH/\hbar}\rho_q e^{-itH/\hbar}\rho_{-q}|\Psi\rangle \tag{20}$$

and the static structure factor

$$S(q) = \int_0^\infty d\omega S(q,\omega) = \frac{1}{N}\langle\Psi|\rho_q\rho_{-q}|\Psi\rangle \tag{21}$$

are independent of the statistics. Quite usefully for the purpose of QMC simulations in configuration space, the un-normalized bosonic ground-state wave function can be written in a Jastrow form for any a [7,32,37]:

$$\Psi_{GS}(r_1 \dots r_N) = \prod_{i<j} |\sin\pi(x_j - x_i)/L|. \tag{22}$$

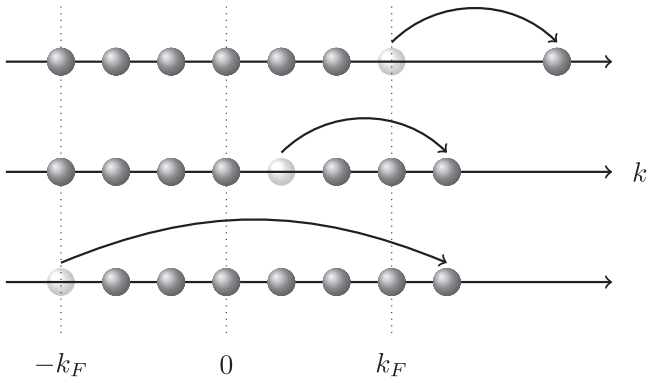

FIG. 1. Pictorial representation of the Lieb-I excitation with $p = 6$ (top) and of the Lieb-II excitation (middle) with $h = 5$ for $N = 7$ HRs. The Lieb-II excitation with $h = 1$ is called umklapp excitation (bottom).

C. Elementary excitations

In the previous section, Sec. II B, we have recalled that the ground-state wave function of the HR system, once expressed in terms of the rod coordinates, has the functional form of a Fermi sea with renormalized coordinates and wave vectors $k_{i,GS}$, specified in terms of integer numbers $n_{i,GS}$. The excited states of the system are obtained creating single or multiple particle-hole pairs on top of this pseudo-Fermi sea [58]. The simplest excitations, illustrated in Fig. 1, consist in the creation of a single particle-hole pair,

$$n_{i,PH} = n_{i,GS} + (p - n_{h,GS})\delta_{i,h}, \tag{23}$$

where $h \in \{1 \dots N\}$ is the index of the original quantum number to be modified ("hole") and $p > n_F$ is the new integer quantum number of index h ("particle"). Among single particle-hole excitations, a role of great importance in the interpretation of $S(q,\omega)$ is played by the following, *Lieb-I*

$$n_{i,I} = n_{i,GS} + (p - n_F)\,\delta_{i,N} \tag{24}$$

and *Lieb-II*

$$n_{i,II} = n_{i,GS} + (n_F + 1 - n_{h,GS})\,\delta_{i,h} \tag{25}$$

modes, which are reminiscent of the corresponding excitations of the Lieb-Liniger model [12]. As shown in Fig. 1, in the Lieb-I excitation, a rod is taken from the Fermi level $h = N$ to some high-energy state associated to an integer $p > n_F$, while in the Lieb-II excitation a rod is taken from a low-energy state h_{II} to just above the Fermi level $p = n_F + 1$. In both cases, in view of the collective nature of the quasi-wave vectors k_i, the excitation of that rod provokes a recoil of all the other rods, according to Eqs. (14) and (15).

A simple calculation shows that the dispersion relation of the Lieb-I excitation is given by

$$E_I^{(N)}(q) = E_I(q) + \Delta E_I^{(N)}(q), \tag{26}$$

where $q \geqslant 0$ is the wave vector of the excitation. The dispersion relation $E_I(q)$ in the thermodynamic limit reads

$$\frac{E_I(q)}{E_F} = \frac{4}{K_L}(x + x^2). \tag{27}$$

In the previous equation $E_F = \frac{\hbar^2 k_F^2}{2m}$, $x = \frac{q}{2k_F}$, and the physical meaning of the Luttinger parameter $K_L = (1-\rho a)^2$ will be elucidated in Sec. II D. Size effects $\Delta E_I^{(N)}(q)$ have the form

$$\frac{\Delta E_I^{(N)}(q)}{E_F} = -\frac{2}{NK_L}\, x\,[1+(1-K_L)x] \tag{28}$$

whenever $\xi^{B,F}(N) = 0$. A similar calculation shows that the dispersion relation of the Lieb-II excitation is given by $E_{II}^{(N)}(q) = E_{II}(q) + \Delta E_{II}^{(N)}(q)$, with $0 \leqslant q \leqslant 2k_F$ and

$$\frac{E_{II}(q)}{E_F} = \frac{4}{K_L}(x - x^2),$$
$$\frac{\Delta E_{II}(q)}{E_F} = \frac{E_{II}(q)}{N} + \frac{x^2}{N}. \tag{29}$$

Other relevant excitations are those producing supercurrent states [9,12,59]

$$n_{i,SC} = n_{i,GS} + s \qquad s \in \mathbb{N} \tag{30}$$

with momenta $q = 2sk_F$ and excitation energies $E_{sc}(q) = \frac{\hbar^2}{2m}\frac{q^2}{N}$ independent of the rod length a and vanishing in the thermodynamic limit. Supercurrent states correspond to Galilean transformations of the ground state with velocities $v_{SC} = \frac{2\hbar k_F}{m}\frac{s}{N}$. The first supercurrent state, in particular, is also termed umklapp excitation [9,12,59].

In the thermodynamic limit, the particle-hole excitations (23) span the region $\omega_-^*(q) \leqslant \omega \leqslant \omega_+^*(q)$ of the (q,ω) plane, where

$$\frac{\hbar\omega_\pm^*(q)}{E_F} = \frac{4}{K_L}\left|\frac{q}{2k_F} \pm \left(\frac{q}{2k_F}\right)^2\right|. \tag{31}$$

The curves $\hbar\omega_\pm^*(q)$ have the same functional form of the ideal Fermi-gas particle-hole boundaries $\hbar\omega_\pm(q) = |\hbar^2 k_F q/m \pm \hbar^2 q^2/2m|$, except for the substitution of the bare mass m with $m^* = mK_L < m$, as we argued in Ref. [28].

The upper branch of this renormalized particle-hole continuum coincides with the Lieb-I mode. For $q \leqslant 2k_F$, its lower branch coincides with the Lieb-II mode and, for $q \geqslant 2k_F$, with the particle-hole excitations

$$n_{i,PH} = n_{i,GS} + 1 + (p - n_{N,GS} - 1)\delta_{i,N}\,, \tag{32}$$

resulting from the combination of the Lieb-I and the umklapp modes.

It is worth noticing that the Lieb-II dispersion relation constitutes the energy threshold for excitations for $0 < q < 2k_F$. Away from this basic region, the energy threshold in the thermodynamic limit can be obtained by a combination of inversions and shifts [52] and corresponds to a combination of a Lieb-II mode and multiple umklapp excitations. To summarize, the low-energy threshold is given by

$$\frac{\hbar\omega_{th}(q)}{E_F} = \frac{4}{K_L}\left[\frac{q_n^*}{2k_F} - \left(\frac{q_n^*}{2k_F}\right)^2\right], \tag{33}$$

where $2nk_F \leqslant q \leqslant 2(n+1)k_F$ and $q_n^* = q - 2nk_F$. Finite-size corrections are the same as in Eq. (29) [28].

Remarkably, (33) corresponds also to the dispersion relation of dark solitons of composite bosons in Yang-Gaudin gases of attractively interacting fermions in the deep molecular regime, even though in that case the molecular scattering length is negative (corresponding to a repulsive Lieb-Liniger molecular gas) [60].

D. Comparison with Luttinger liquid theories

The low-energy excitations of a broad class of interacting 1D systems are captured by the phenomenological TLL field theory [3,47–51]. The TLL provides a universal description of interacting Fermi and Bose particles by introducing two fields, $\phi(x)$ and $\theta(x)$, representing the density and phase oscillations of the destruction operator $\Psi(x) \simeq \sqrt{\rho + \partial_x\phi(x)}e^{i\theta(x)}$, and a quadratic low-energy Hamiltonian describing the dynamics of those fields,

$$H_{LL} = \frac{\hbar}{2\pi}\int dx\left(cK_L\partial_x\theta(x)^2 + \frac{c}{K_L}\partial_x\phi(x)^2\right). \tag{34}$$

For Galilean-invariant systems, the sound velocity c is related to the positive Luttinger parameter K_L through $c = \frac{v_F}{K_L}$. The quadratic nature of (34) allows for the calculation of correlation functions and thermodynamic properties in terms of c and K_L. Within the TLL theory, in the low-momentum and low-energy regime $S(q,\omega)$ features collective phononlike excitations $\omega_{LL}(q) = c|q|$ with sound velocity c.

The TLL theory has been recently extended [3,52] beyond the low-energy limit, where the assumption of a linear excitation spectrum $\omega_{LL}(q)$ is not sufficient for accurately predicting dynamic response functions. Assuming that, for any momentum q, $S(q,\omega)$ has support above a low-energy threshold $\omega_{th}(q)$ and interpreting excitations with momentum q between $2nk_F$ and $2nk_F + 2k_F$ as the creation of mobile holes of momentum $q_n^* = q - 2nk_F$ coupled with the TLL [3,52], it is possible to show that for a broad class of Galilean-invariant systems $S(q,\omega)$ features a power-law singularity close to the low-energy threshold $\omega_{th}(q)$ with the following functional form:

$$S(q,\omega) = \theta[\omega - \omega_{th}(q_n^*)]\,|\omega - \omega_{th}(q_n^*)|^{-\mu_n(q)}\,, \tag{35}$$

where the exponent

$$\mu_n(q) = 1 - \frac{1}{2}\left((2n+1)\sqrt{K_L} + \frac{\delta_+(q_n^*) + \delta_-(q_n^*)}{2\pi}\right)^2 - \frac{1}{2}\left(\frac{1}{\sqrt{K_L}} + \frac{\delta_+(q_n^*) - \delta_-(q_n^*)}{2\pi}\right) \tag{36}$$

is specified in terms of the phase shifts

$$\frac{\delta_\pm(q)}{2\pi} = \frac{\frac{1}{\sqrt{K_L}}\left(\frac{\hbar q}{m} + \frac{\partial\omega_{th}(q)}{\partial q}\right) \pm \sqrt{K_L}\left(\frac{v_s}{K_L} - \frac{1}{\pi}\frac{\partial\omega_{th}(q)}{\partial\rho}\right)}{2\left(\mp\frac{\partial\omega_{th}(q)}{\partial q} - v_s\right)}. \tag{37}$$

The only phenomenological inputs required by the nonlinear TLL theory are the Luttinger parameter K_L and the low-energy threshold $\omega_{th}(q)$, which in the case of hard rods are exactly known. Namely, we recall that the Luttinger parameter K_L [50,51] can be computed from the compressibility

$$\kappa_S^{-1} = \rho\,\frac{\partial}{\partial\rho}\left(\rho^2\,\frac{\partial E_\infty}{\partial\rho}\right) \tag{38}$$

through the formula $mK_L^2 = \hbar^2 k_F^2\,\rho\,\kappa_S$. The resulting exact expression, $K_L = (1-\rho a)^2$ [32], provides a Luttinger

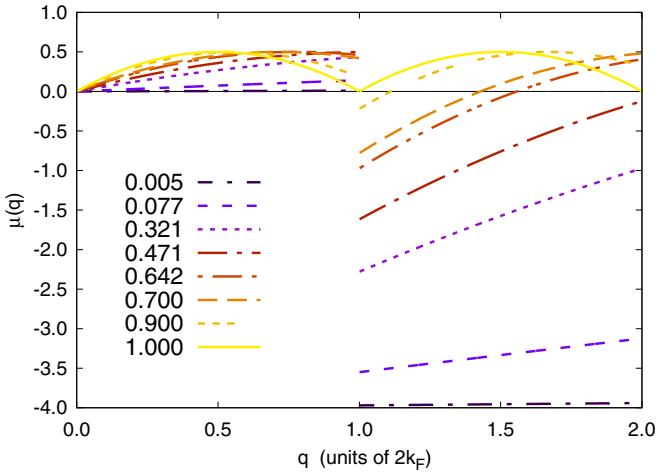

FIG. 2. Nonlinear Luttinger theory exponents $\mu(q)$ for hard rods at the studied densities from $\rho a = 0.077$ (blue solid line) to $\rho a = 0.900$ (red solid line). Momenta are measured in units of $2k_F = 2\pi\rho$. The $\rho a \to 1$ limit is also shown (solid line). Notice that the densities $\rho a \geqslant 0.5$ have a special wave vector $\mathcal{Q}_1$ between $2k_F$ and $4k_F$.

parameter always smaller than 1, and converging towards 0 as the excluded volume Na converges towards L. Notice that both Lieb-I and Lieb-II dispersions approach $q = 0$ with slope equal to the sound velocity $c = \frac{v_F}{K_L} > v_F$. The low-energy threshold, Eq. (33), has been described in the previous section.

Knowledge of these two quantities permits us to compute the exponent $\mu_n(q)$ exactly from (36) and (37). We find [28]

$$\mu_n(q) = -2(\tilde{q} - n)\,[\tilde{q} - (n+1)]\,, \tag{39}$$

with $\tilde{q} = \frac{qa}{2\pi}$. In Fig. 2 we show the power-law exponents for momenta $0 < q < 4k_F$ and different densities. Notice that the functional form of (39) is that of a sequence of parabola arcs, intersecting null values at the special momenta $\mathcal{Q}_n = n2\pi/a$, with integer $n < \rho a/(1-\rho a)$. Such momenta, even for larger n, have already been recognized to be special [32] in that they admit the exact calculation of $S(\mathcal{Q}_n)$ and $S(\mathcal{Q}_n,\omega)$. Namely, for those special momenta, the HRs at density ρ behave as an ideal Fermi gas with increased density $\rho' = \rho/(1-\rho a)$.

It is worth pointing out that TLL theories have limits of applicability and thus do not exhaust our understanding of 1D substances [27,61,62]. The investigation of dynamical properties like $S(q,\omega)$ beyond the limits of applicability of Luttinger liquid theories, where the physics is nonuniversal, typically requires numerical calculations or QMC simulations [28,61,63].

III. METHODS

In the present work, the zero-temperature dynamical structure factor of a system of Bose HRs is calculated using the *exact* path integral ground state (PIGS) QMC method to compute imaginary-time correlation functions of the density fluctuation operator, and the state-of-the-art genetic inversion via falsification of theories (GIFT) analytic continuation method to extract the dynamical structure factor.

This approach, which we briefly review in this section, has provided robust calculations of dynamical structure factors for several nonintegrable systems such as 1D, 2D, and 3D He atoms [28,41,64,65] and hard spheres [66].

The PIGS method is a projection technique in imaginary time that, starting from a trial wave function $\Psi_T(R)$, where $R = (r_1 \ldots r_N) \in \mathcal{C}$ denotes a set of spatial coordinates of the N particles, projects it onto the ground-state wave function $\Psi_{GS}(R)$ after evolution over a sufficiently long imaginary-time interval τ [38–40]. In typical situations, the functional form of $\Psi_T(R)$ is guessed by combining physical intuition and mathematical arguments based on the theory of stochastic processes [67]. $\Psi_T(R)$ is then specified by one or more free parameters that are chosen using suitable optimization algorithms [68–70].

In the case of HRs, knowledge of the exact ground-state wave function (22) makes the projection of a trial wave function $\Psi_T(R)$ approximating the ground state of the system unnecessary. However, the PIGS method can be used to give unbiased estimates of the density-density correlator

$$\begin{aligned} F(q,\tau) &= \langle \Psi_{GS}|e^{\tau H}\rho_{-q}\,e^{-\tau H}\,\rho_q|\Psi_{GS}\rangle \\ &= \frac{\int dR_M dR_0\; p(R_M,R_0)\,\rho_{-q}(R_M)\,\rho_q(R_0)}{\int dR_M dR_0\; p(R_M,R_0)}\,, \end{aligned} \tag{40}$$

with $p(R_M,R_0) = \Psi_{GS}(R_M)G(R_M,R_0;\tau)\Psi_{GS}(R_0)$ and $G(R_M,R_0;\tau) = \langle R_M|e^{-\tau H}|R_0\rangle$.

The propagator $G(R',R;\tau)$ is in general unknown, but suitable approximate expressions are available for small $\delta\tau = \tau/M$, where M is a large integer number. Using one of these expressions in place of the exact propagator is the only approximation characterizing the calculations of the present work. The method is exact though, since this approximation affects the computed expectation values to an extent which is below their statistical uncertainty, and such a regime is always attainable by taking $\delta\tau$ sufficiently small. Then, the convolution formula permits us to express $G(R_M,R_0;\tau)$ as

$$G(R_M,R_0;\tau) = \int dR_{M-1}\ldots dR_1 \prod_{i=0}^{M-1} G(R_{i+1},R_i;\delta\tau)\,, \tag{41}$$

from which the PIGS estimator of $F(q,\tau)$ takes the form

$$F(q,\tau) = \frac{\int dX\; p(X)\,\rho_{-q}(R_M)\,\rho_q(R_0)}{\int dX\; p(X)}\,. \tag{42}$$

In (42), $X = (R_0 \ldots R_M)$ denotes a path in the configuration space $\mathcal{C}$ of the system, and

$$p(X) = \Psi_{GS}(R_M)\prod_{i=0}^{M-1} G(R_{i+1},R_i;\delta\tau)\Psi_{GS}(R_0) \tag{43}$$

can be efficiently sampled using the Metropolis algorithm [71]. In the present work, we have employed the pair-product approximation [72] to express the propagator relative to a small time step $\delta\tau$ as

$$G(R,R';\delta\tau) = \prod_{i=1}^{N} G_0(r_i,r_i';\delta\tau)\prod_{i<j}^{N} G_{\rm rel}(r_{ij},r_{ij}';\delta\tau)\,, \tag{44}$$

TABLE I. Densities studied in the present work, corresponding values of K_L, and adopted time steps in units of $1/E_F(\rho)$.

ρa	K_L	$\delta\tau$
0.005	0.990	0.0025
0.077	0.852	0.0176
0.321	0.461	0.0509
0.471	0.280	0.0219
0.642	0.128	0.0142
0.700	0.090	0.0097
0.900	0.010	0.0012

where G_0 is the free-particle propagator

$$G_0(r,r';\delta\tau) = \frac{1}{\sqrt{2\pi\lambda\delta\tau}} e^{-(r-r')^2/4\lambda\delta\tau} \tag{45}$$

with $\lambda = \hbar^2/2m$, and $G_{\rm rel}$ is obtained from the exactly known solution of the two-body scattering problem, similarly to a standard approach for hard spheres in 3D [73],

$$G_{\rm rel}(r,r';\delta\tau) = 1 - e^{-\frac{(r-a)(r'-a)}{2\lambda\delta\tau}}. \tag{46}$$

Moreover, in order to select an appropriately small $\delta\tau$, we have checked both the convergence of the static structure factor and the convergence of energy when the exact initial trial wave function is replaced with an approximate one [74]. See Table I for a summary of the time steps employed in our PIGS simulations.

The initial imaginary-time value of Eq. (40) is the static structure factor $F(q,0) = S(q)$. For finite values of τ, $F(q,\tau)$ is instead related to $S(q,\omega)$ by the Laplace transform

$$F(q,\tau) = \int_0^\infty d\omega\, e^{-\tau\omega}\, S(q,\omega)\,. \tag{47}$$

Equation (47) should be inverted in order to determine $S(q,\omega)$ from $F(q,\tau)$. However, it is well known that such an inverse problem is *ill-posed*, in the sense that many different trial dynamical structure factors, ranging from featureless to rich-in-structure distributions, have a forward Laplace transform which is compatible with the QMC results for $F(q,\tau)$; there is not enough information to find a unique solution of (47) [41,75–80]. Different methodologies have been used to extract real frequency response functions from imaginary-time correlators; in the present work, we rely on the GIFT method [41]. The aim of GIFT is to collect a large collection of such dynamical structure factors in order to discern the presence of common features (e.g., support, peak positions, intensities, and widths). The GIFT method has been applied to the study of liquid ^{4}He [28,81,82], 3D hard spheres [66], 2D Yukawa Bosons [83], liquid ^{3}He [64], 2D soft disks [84,85], the 2D Hubbard model [86], and 1D soft rods [87], in all cases providing very accurate reconstructions of $S(q,\omega)$ or the single-particle spectral function. Recently [28], we have shown that in 1D, when $\omega_{th}(q)$ is known, also the shape close to the frequency threshold can be approximately inferred. This is the reason why in Sec. II C we insisted on the calculation of $\omega_{th}(q)$ for a finite system, which is a most useful quantity in our approach. Details of the GIFT method can be found in [28,41]. As in [28], we have used genetic operators which are able to better describe broad features typical of 1D systems. Moreover, the set of discrete frequencies of the model spectral functions used in the algorithm has been extended to nonequispaced frequencies in order to better describe the regions where most of the weight accumulates.

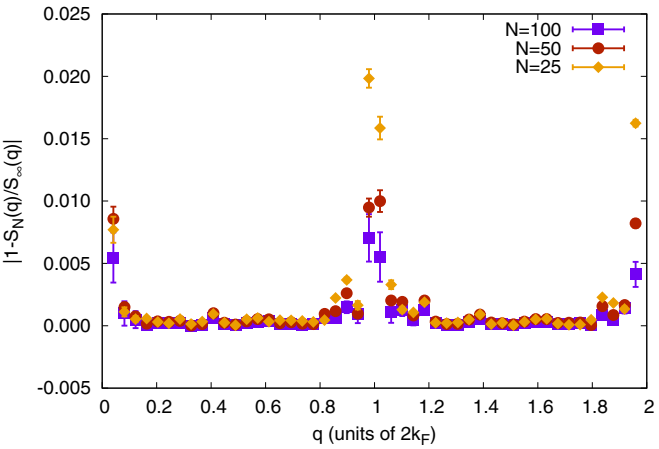

FIG. 3. We quantify the finite-size effects on $S(q)$ at the representative density $\rho a = 0.700$ computing the relative error $|S_N(q) - S_\infty(q)|/S_\infty(q)$, where $S_\infty(q) = \lim_{N\to\infty} S_N(q)$ is extrapolated. Away from the points $q = 2k_F, 4k_F$, the relative error is below 1% for $N = 50$ particles.

IV. RESULTS

We computed $F(q,\tau)$ for systems of $N = 50$ hard rods at densities ρa listed in Table I, and wave vectors $q \leqslant 8k_F$. Before describing our results on the dynamical structure factor, we demonstrate the accuracy of our calculations by analyzing in detail finite-size effects on static properties which have already been studied in Ref. [32].

A. Assessment of accuracy

Results are affected by very weak finite-size effects and thus are well representative of the thermodynamic limit. For example, (17) and (18) yield the following finite-size corrections to the ground-state energy:

$$\frac{E_{GS}}{N} = E_\infty\left(1 - \frac{1}{N^2}\right) \tag{48}$$

where $\frac{E_{GS}}{50} = 0.999\,6\,E_\infty$. To further assess the finite-size effects on our results, in Fig. 3 we compute the static structure factor of $N = 50, 100$ hard rods at $\rho a = 0.700$ using the VMC method, which is an exact method when the exact (ground-state) wave function is known, as in this case.

At $q = 2k_F, 4k_F$, the static structure factor displays peaks of diverging weight as predicted by the TLL theory [32,88]:

$$\begin{aligned} S(2mk_F) &= S_{smooth}(2mk_F) + S_{peak}(2mk_F) \\ &= S_{smooth}(2mk_F) + C_m\, N^{1-2m^2K_L}\,. \end{aligned} \tag{49}$$

Away from those points, the VMC estimates of the static structure factor are compatible with each other and with the extrapolation of $S(q)$ to the thermodynamic limit, within the error bars of the simulations, reflecting the weakness of

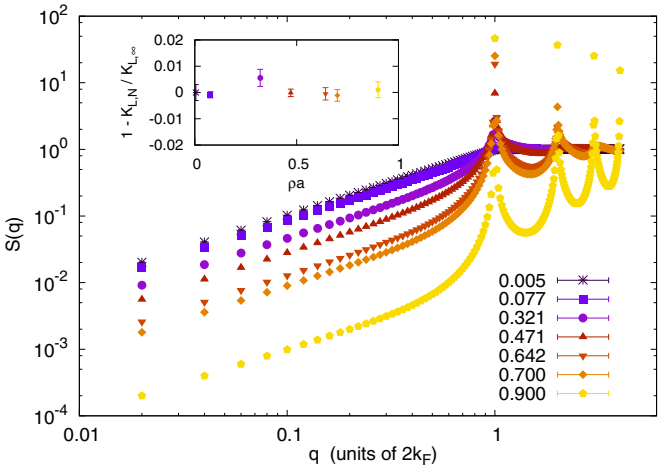

FIG. 4. Static structure factor of $N = 50$ rods at $\rho a = 0.005, 0.077, 0.321, 0.471, 0.642, 0.700, 0.900$. Inset: Relative error on the Luttinger parameter, computed from the low-momentum behavior of the static structure factor $S(q) \simeq K_L q/(2k_F)$. In all cases, the relative error is below 1%.

finite-size effects. Moreover, in Fig, 4 we show that static structure factors of $N = 50$ rods permit us to compute the Luttinger parameter K_L without appreciable finite-size effects.

The same favorable behavior is exhibited by $F(q,\tau)$. In Fig. 5, we show $F(q,\tau)$ for $N = 50, 100$ rods at the representative density $\rho a = 0.700$. Away from $q = 2k_F$ the two systems have statistically compatible $F(q,\tau)$, confirming the modest entity of finite-size effects.

B. Dynamical structure factors

In Fig. 6 we show the dynamical structure factor at densities ranging from $\rho a = 0.005$ to 0.900. At all the studied densities, for momentum $q < 2k_F$, $S(q,\omega)$ has most of the

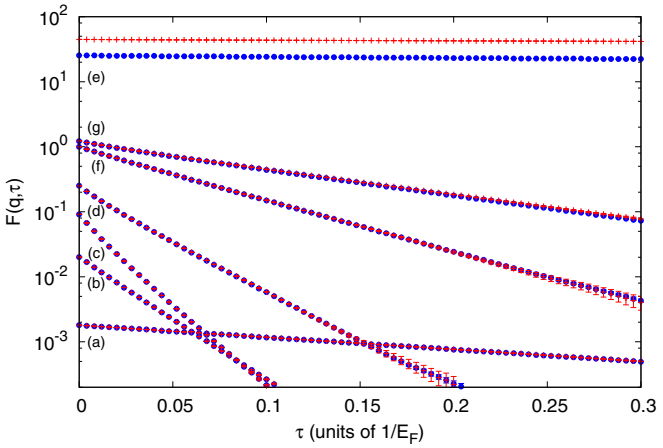

FIG. 5. $F(q,\tau)$ of $N = 50, 100$ (blue circles, red open diamonds) rods at $\rho a = 0.700$ for $\frac{q}{2k_F} = 0.02, 0.22, 0.62, 0.82, 0.96, 1.00, 1.08$ (a to g). At $q = 2k_F$ we observe strong finite-size effects, originating from the quasi-Bragg peaks in $S(q)$. Away from $q = 2k_F$, in the relevant imaginary-time interval $\tau E_F \leqslant 0.3$ the two $F(q,\tau)$ are in satisfactory agreement.

spectral weight inside the particle-hole band $\omega^*_-(q) \leqslant \omega \leqslant \omega^*_+(q)$ spanned by single particle-hole excitations [Eq. (31)]. Contributions from multiple particle-hole excitations become relevant at high densities and momenta.

At the lowest density, panel (a), the spectral weight is broadly distributed inside the particle-hole band, showing a behavior reminiscent of the Tonks-Girardeau model of impenetrable pointlike bosons, to which the HR model reduces in the $\rho a \to 0$ limit.

The low momentum and energy behavior can be understood in the light of the nonlinear TLL theory. As illustrated in Fig. 2, for momenta $q < 2k_F$ it predicts a power-law behavior for $S(q,\omega)$, with an exponent (39) slightly larger than zero. This prediction is consistent with the spectrum in panel (a), showing a weak concentration of spectral weight close to the low-energy threshold for $q < 2k_F$. For $q > 2k_F$, the support of $S(q,\omega)$ departs from the low-energy threshold, as it can be seen in panel (a), where the spectral weight remains concentrated inside the particle-hole band for all q. Correspondingly, for $2k_F < q < 4k_F$, the nonlinear TLL predicts a large negative exponent, suggesting the absence of spectral weight in the proximity of the low-energy threshold.

A similar behavior is shown at density $\rho a = 0.077$, panel (b), where the spectral weight concentrates more pronouncedly at the low-energy threshold for $q < 2k_F$. This is again in agreement with the nonlinear TLL theory, predicting a larger negative exponent $\mu(q)$.

The dynamical structure factors in panels (a), (b) are also in qualitative agreement with numeric calculations for the super Tonks-Girardeau gas, for which $0.4 \lesssim K_L < 1$ [57]; in fact, we verified that the spectra shown in Ref. [57] manifest a low-energy support at positive energy, which is compatible with Eq. (33), up to $\rho a \simeq 0.1$ (even though one should remark that a negative-frequency component is also present due to the excited nature of the super Tonks-Girardeau state).

The spectra in Fig. 6 show that the Feynman approximation

$$\hbar\omega_{FA}(q) = \frac{\hbar^2 q^2}{2m S(q)} \tag{50}$$

breaks down beyond $\frac{q}{2k_F} \simeq 0.1$. Interestingly, around $\frac{q}{2k_F} \simeq 0.1$ also the approximation of $\omega_{th}(q)$ with a linear function of q ceases to be adequate. The simultaneous appearance of nonlinear terms in $\omega_{th}(q)$ and corrections to the Feynman approximation in $S(q,\omega)$ are in fact deeply related phenomena, as explained by the nonlinear TLL theory.

When $K_L < 1/2$, Eq. (49) indicates that a peak manifests in the static structure factor at $q = 2k_F$. This change in behavior is also reflected in $S(q,\omega)$, as shown in panels (c) and (d). The spectral weight concentrates close to the lower branch $\omega^*_-(q)$ of the particle-hole band, in a region of dense spectral weight that we call the lower mode following [28], where a similar behavior was observed in 1D ^{4}He at high density. In both HRs and ^{4}He, above the lower mode stretches a high-energy structure gathering a smaller fraction of spectral weight. Such a high-energy structure has a minimum at $q = 2k_F$, close to the free-particle energy $E = 4E_F$, and is symmetric around $q = 2k_F$ [see panel (d) in Fig. 6].

Panel (d) also shows that, as K_L decreases below 1/2, the support of $S(q,\omega)$ extends below $\omega^*_-(q)$ for $q > 2k_F$,

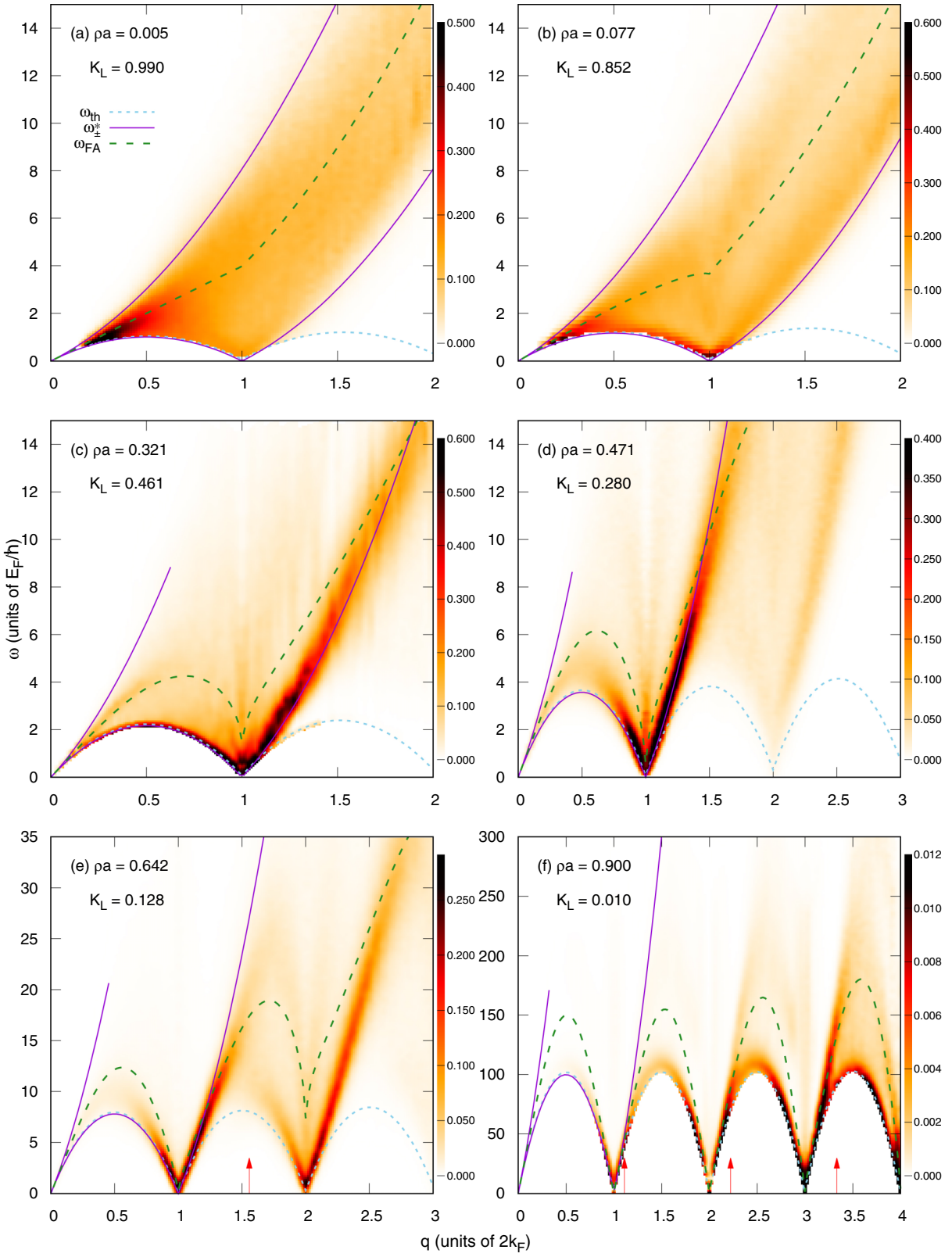

FIG. 6. Color map of the dynamic structure factor, in units of $\hbar/E_F$, at $\rho a = 0.005, 0.077, 0.321, 0.471, 0.642, 0.900$ (left to right, top to bottom). Momenta are measured in units of $2k_F = 2\pi\rho$ and energies in units of E_F. The low-energy threshold (blue dotted line), the branches $\omega^*_\pm(q)$ (purple solid lines), and the Feynman approximation for the excitation spectrum (green dashed line) are drawn for comparison. Panels (e), (f) also show the special wave vectors $\mathcal{Q}_n$ (red arrows).

still remaining above $\omega_{th}(q)$. In the high-density regime $\rho a \geqslant 0.642$, such a region of a momentum-energy plane hosts some of the most remarkable properties of $S(q,\omega)$, as it can be read from panel (e), where the shape of $S(q,\omega)$ changes considerably for $2k_F < q < 4k_F$.

For $q < 2.8k_F$, the spectral weight concentrates in a narrow region of the momentum-energy plane that gradually departs from the low-energy threshold. For $2.8k_F < q < 3.6k_F$, $S(q,\omega)$ suddenly and considerably broadens and flattens. Finally, for $3.6k_F < q < 4k_F$, the spectral weight again concentrates close to the low-energy threshold. This highly nontrivial behavior is in qualitative agreement with the nonlinear Luttinger liquid theory, predicting a negative exponent for $q < \mathcal{Q}_1$, where $\frac{\mathcal{Q}_1}{2k_F} = \frac{1}{a\rho} = 1.558$. At $q = \mathcal{Q}_1$ the nonlinear Luttinger liquid theory predicts a flat dynamical structure factor close to the low-energy threshold, in agreement with an exact prediction by Mazzanti *et al.* [32] and with our observations for the 1D HR system, but also for a 1D system of ^{4}He atoms [28]. Beyond $\mathcal{Q}_1$ the nonlinear Luttinger liquid theory predicts a positive exponent and we observe the spectral weight concentrating close to the low-energy threshold, as for $q < 2k_F$. Notice that, although the condition for having quasi-Bragg peaks is $K_L < 1/2$, the first special momentum with a flat spectrum appears only for $\rho a > 1/2$, namely, $K_L < 1/4$, since one must have $\mathcal{Q}_1 = 2\pi/a < 4\pi\rho$.

It is well known [31,32] that, in the high-density regime $K_L \ll 1$, HRs show up in a packing order leading to a quasisolid phase, crystallization being prohibited by the reduced dimensionality and by the range of the interaction. The emergence of the quasisolid phase is signaled by the peaks of the static structure factor that approach linear growth with the system size, a peculiar prerogative of the Bragg peaks, only in the $\rho a \to 1$ limit.

As far as $S(q,\omega)$ is concerned, the increase of the density transfers spectral weight to the low-energy threshold at wave vectors $q = 2k_F, 4k_F$. We interpret this phenomenon as revealing that $S(q,\omega)$ is gradually approaching translational invariance $q \to q + 2k_F$ in the variable q. This conjecture is corroborated by the observation that, as the density is further increased, the exponent $\mu_n(q)$ pointwise converges to the periodic function:

$$\mu_n(q) = -2\left(\frac{q}{2k_F} - n\right)\left(\frac{q}{2k_F} - (n+1)\right), \qquad (51)$$

with $2nk_F \leqslant q \leqslant 2(n+1)k_F$ (illustrated in Fig. 2). In this respect, it is interesting to observe panel (f) of Fig. 6, showing the dynamical structure factor of HRs at $\rho a = 0.900$. For $q < 8k_F$, the spectral weight almost always concentrates around $\omega_{th}(q)$, except in the small ranges of wave vectors $2nk_F < q < \mathcal{Q}_n$. This makes $S(q,\omega)$ resemble the dispersion relation of longitudinal phonons of a monoatomic chain, in this range of momenta. However, the noncommensurability of $\mathcal{Q}_1$ with $2k_F$ renders the spectrum only quasiperiodic, a behavior which is more and more manifest at higher momenta. To analyze this intriguing regime in more detail, we have reconstructed the spectra at $\rho a = 0.900$ up to $q = 38k_F$. The results are shown in Fig. 7 and indicate a crucial role of the reduced-size ideal Fermi gas in drawing large-scale momentum and frequency boundaries for the HR spectrum. If we define the

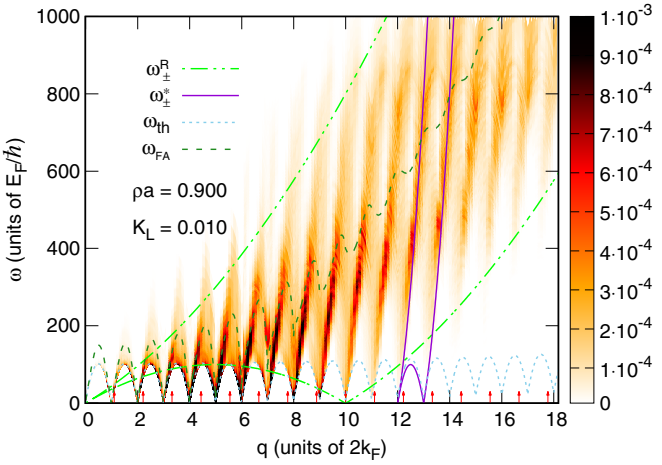

FIG. 7. Color map of the dynamic structure factor at $\rho a = 0.900$ on a much larger momentum and frequency scale than in Fig. 6(f). Units and reference curves are the same as in Fig. 6. The special wave vectors $\mathcal{Q}_n$ (red arrows) are shown by long (red) arrows. The role of both the HR renormalized particle-hole frequencies (solid curves) and of the reduced-volume ideal Fermi-gas band (dot-dashed curves) are shown.

density $\rho' = \rho/(1-\rho a)$, we observe that above $q = 20k_F = 2\pi\rho'$, namely, twice the Fermi momentum of the reduced-size IFG, the spectrum is never peaked along the low-energy HR threshold; however, it presents a stripe structure, repeating the Lieb-I mode plus multiple umklapp excitations, and becoming again flat at momenta $\mathcal{Q}_n$. At the level of accuracy of our GIFT reconstructions, the stripes are bounded by the particle-hole band of the reduced-size IFG:

$$\hbar\omega^R_{\pm}(q) = \frac{\hbar^2}{2m}|2\pi\rho' q \pm q^2|\,. \qquad (52)$$

To corroborate this observation, we find that the special momenta $\mathcal{Q}_n$ also analytically correspond to the crossings of the lower reduced-size IFG boundary and the HR threshold

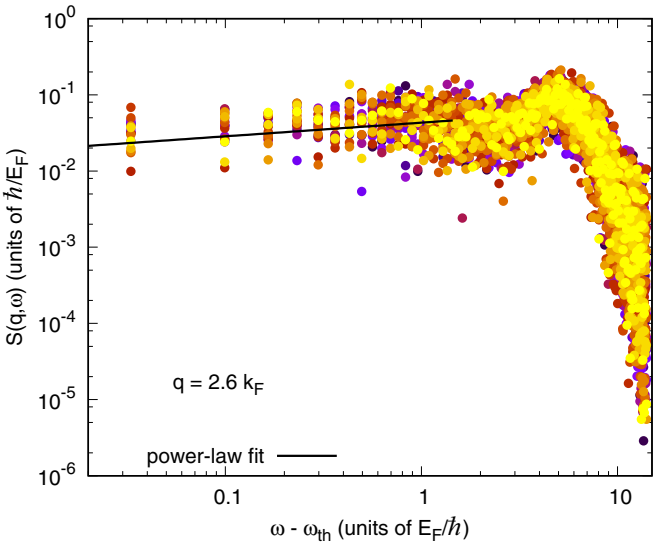

FIG. 8. Power-law fit of reconstructed spectra for $\rho a = 0.700$ and $q = 2.6k_F$. The fitted exponent is $\mu = -0.18(3)$, which is compatible with the analytical prediction (51) that yields $\mu = -0.196$.

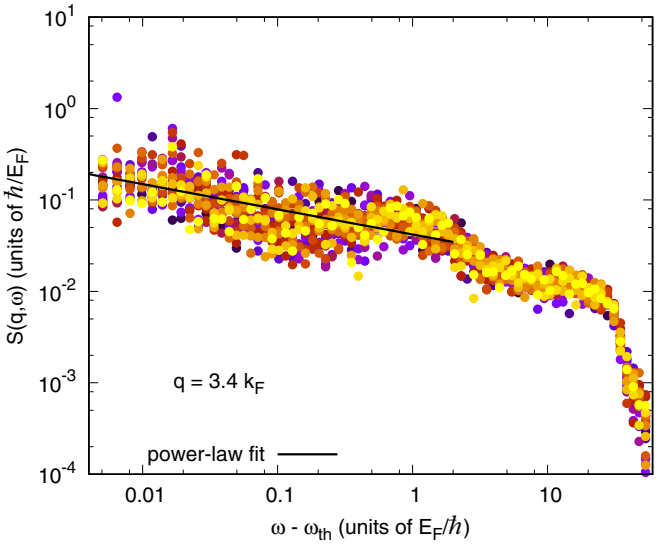

FIG. 9. Power-law fit of reconstructed spectra for $\rho a = 0.700$ and $q = 3.4k_F$. The fitted exponent is $\mu = 0.28(3)$, which is compatible with the analytical prediction (51) that yields $\mu = 0.308$.

(for $q < 2\pi\rho'$) or the HR repeated Lieb-I modes ($q > 2\pi\rho'$). It is tempting to conclude that the HR spectrum can be almost completely described by the synergy of two rescaled ideal Fermi gases: one with the same density, but renormalized mass $m^* = mK_L$, the other with the same mass, but increased density $\rho' = \rho/K_L^{1/2}$. Only in the unphysical $\rho a \to 1$ limit, therefore, $S(q,\omega)$ would attain the translational invariance observed, for instance, in half-filled Hubbard chains with strong on-site repulsion [89,90].

Finally, in discussing Fig. 6, we stressed on multiple occasions that low-energy properties of $S(q,\omega)$ are captured by the nonlinear TLL theory. Following the approach of [28], in Figs. 8 and 9 we show that the agreement is quantitative, focusing on density $\rho a = 0.700$ and two momenta close to $\mathcal{Q}_1$, representative of negative and positive power-law exponents, and fitting multiple spectral reconstructions with the functional form given by Eq. (35). The agreement with the analytical expression for the power-law exponent (39) is good, even though the accuracy is strongly dependent on the quality of the original $F(q,\tau)$ and it is particularly delicate to fit the spectra when the spectrum goes to zero close to the threshold.

V. CONCLUSIONS AND OUTLOOK

We have computed the zero-temperature dynamical structure factor of one-dimensional hard rods by means of state-of-the-art QMC and analytic continuation techniques. By increasing the rod length, the dynamical structure factor reveals a transition from the Tonks-Girardeau gas, to a super Tonks-Girardeau regime and finally to a quasi-solid regime.

The low-energy properties of the dynamical structure factor are in qualitative agreement with the nonlinear LL theory. However, the methodology provides a quantitative estimation of the dynamical structure factor also in the high-energy regime, lying beyond the reach of LL theories. Our study reveals strong similarities between the dynamical structure factor of HRs and 1D ^{4}He at linear densities $\rho \geqslant 0.150$ Å^{-1} [28], extending to the high-energy regime (well above the low-energy threshold). In particular, both systems show a flat dynamical structure factor in correspondence with the wave vectors $\mathcal{Q}_n$, in agreement with a previous theoretical prediction [32], and feature a high-energy structure overhanging the lower mode around the umklapp point $q = 2k_F$. We have also unveiled a peculiar structure of the spectrum in the high-density and high-momentum regime, which can be described in terms of the particle-hole boundaries of two renormalized ideal Fermi gases.

At this point we want to remark that an intriguing feature of 1D ^{4}He (and arguably of all 1D quantum liquids which admit a two-body bound state) is that its Luttinger parameter K_L spans all positive values $0 < K_L < \infty$ as the linear density is increased [28], not only the $K_L \leqslant 1$ regime, as in the case of HR or dipolar systems [91]. This is due to the attractive tail of the interaction potential, which dominates at low density. Such a feature also has to be contrasted to the repulsive Lieb-Liniger model, for which one obtains $1 \leqslant K_L \leqslant \infty$ by tuning the interaction strength. Finally, also the Calogero-Sutherland model reproduces all possible K_L, however by tuning interaction only [92].

We hope the present work will encourage further experimental research in 1D systems with volume exclusion effects and theoretical investigation of the HR model. Our results may be relevant also for the linear response dynamics of resonant Rydberg gases in 1D configurations [93]. On the theoretical side, possible directions for further developments might be the alternative calculations of $S(q,\omega)$, based, e.g., on the VMC evaluation of the matrix elements of ρ_q and/or the calculation of finite-temperature equilibrium and dynamical properties.

ACKNOWLEDGMENTS

We acknowledge useful discussions with G. Astrakharchik. We thank M. Panfil and coauthors for providing us with their data on the super Tonks-Girardeau gas [57]. We acknowledge the CINECA awards IsC29-SOFTDYN and IsC32-EleMEnt, and CINECA and Regione Lombardia LISA award LI05p-PUMAS, for the availability of high-performance computing resources and support. We also acknowledge computing support from the computational facilities at the College of William and Mary and at the Physics Department of the University of Milan. M.M. and E.V. acknowledge support from the Simons Foundation and NSF through Grant No. DMR-1409510. M.R. acknowledges the EU Horizon 2020-FET QUIC 641122 project for funding. G.B. acknowledges support from the University of Milan through Grant No. 620, Linea 2 (2015).

[1] T. Giamarchi, *Quantum Physics in One Dimension* (Oxford University Press, Oxford, UK, 2004).

[2] M. A. Cazalilla, R. Citro, T. Giamarchi, E. Orignac, and M. Rigol, Rev. Mod. Phys. **83**, 1405 (2011).

[3] A. Imambekov, T. L. Schmidt, and L. I. Glazman, Rev. Mod. Phys. **84**, 1253 (2012).
[4] P. C. Hohenberg, Phys. Rev. **158**, 383 (1967).
[5] N. D. Mermin and H. Wagner, Phys. Rev. Lett. **17**, 1133 (1966).
[6] S. Coleman, Commun. Math. Phys. **31**, 259 (1973).
[7] M. Girardeau, J. Math. Phys. **1**, 516 (1960).
[8] L. Pitaevskii and S. Stringari, Phys. Rev. B **47**, 10915 (1993).
[9] G. F. Giuliani and G. Vignale, *Quantum Theory of the Electron Liquid* (Cambridge University Press, Cambridge, UK, 2005).
[10] T. Nagamiya, Proc. Phys.-Math. Soc. Japan **22**, 705 (1940).
[11] E. H. Lieb and W. Liniger, Phys. Rev. **130**, 1605 (1963).
[12] E. H. Lieb, Phys. Rev. **130**, 1616 (1963).
[13] B. Sutherland, Phys. Rev. A **4**, 2019 (1971).
[14] B. Sutherland, J. Math. Phys. **12**, 251 (1971).
[15] B. Sutherland, Phys. Rev. B **38**, 6689 (1988).
[16] B. Paredes, A. Widera, V. Murg, O. Mandel, S. Fölling, I. Cirac, G. V. Shlyapnikov, T. W. Hänsch, and I. Bloch, Nature (London) **429**, 277 (2004).
[17] T. Kinoshita, T. Wenger, and D. S. Weiss, Science **305**, 1125 (2004).
[18] E. Haller, M. Gustavsson, M. J. Mark, J. G. Danzl, R. Hart, G. Pupillo, and H.-C. Nägerl, Science **325**, 1224 (2009).
[19] H. P. Stimming, N. J. Mauser, J. Schmiedmayer, and I. E. Mazets, Phys. Rev. Lett. **105**, 015301 (2010).
[20] M. Kuhnert, R. Geiger, T. Langen, M. Gring, B. Rauer, T. Kitagawa, E. Demler, D. Adu Smith, and J. Schmiedmayer, Phys. Rev. Lett. **110**, 090405 (2013).
[21] S. Hofferberth, I. Lesanovsky, B. Fischer, T. Schumm, and J. Schmiedmayer, Nature (London) **449**, 324 (2007).
[22] T. Langen, R. Geiger, M. Kuhnert, B. Rauer, and J. Schmiedmayer, Nat. Phys. **9**, 640 (2013).
[23] E. Witkowska, P. Deuar, M. Gajda, and K. Rzazewski, Phys. Rev. Lett. **106**, 135301 (2011).
[24] T. Karpiuk, P. Deuar, P. Bienias, E. Witkowska, K. Pawlowski, M. Gajda, K. Rzazewski, and M. Brewczyk, Phys. Rev. Lett. **109**, 205302 (2012).
[25] V. Guarrera, D. Muth, R. Labouvie, A. Vogler, G. Barontini, M. Fleischhauer, and H. Ott, Phys. Rev. A **86**, 021601 (2012).
[26] J. P. Ronzheimer, M. Schreiber, S. Braun, S. S. Hodgman, S. Langer, I. P. McCulloch, F. Heidrich-Meisner, I. Bloch, and U. Schneider, Phys. Rev. Lett. **110**, 205301 (2013).
[27] N. Fabbri, M. Panfil, D. Clément, L. Fallani, M. Inguscio, C. Fort, and J. S. Caux, Phys. Rev. A **91**, 043617 (2015).
[28] G. Bertaina, M. Motta, M. Rossi, E. Vitali, and D. E. Galli, Phys. Rev. Lett. **116**, 135302 (2016).
[29] J. V. Pearce, M. A. Adams, O. E. Vilches, M. R. Johnson, and H. R. Glyde, Phys. Rev. Lett. **95**, 185302 (2005).
[30] M. Mercedes Calbi, M. W. Cole, S. M. Gatica, M. J. Bojan, and G. Stan, Rev. Mod. Phys. **73**, 857 (2001).
[31] F. Mazzanti, G. E. Astrakharchik, J. Boronat, and J. Casulleras, Phys. Rev. A **77**, 043632 (2008).
[32] F. Mazzanti, G. E. Astrakharchik, J. Boronat, and J. Casulleras, Phys. Rev. Lett. **100**, 020401 (2008).
[33] J. D. van der Waals, *The Equation of State for Gases and Liquids*, Nobel Lectures in Physics, Vol. 1 - 1901–1921 (World Scientific Publishing Co Pte Ltd., Singapore, 1998), pp. 254–265.
[34] J. H. Jeans, *The Dynamical Theory of Gases* (Cambridge University Press, Cambridge, UK, 1916).
[35] L. Tonks, Phys. Rev. **50**, 955 (1936).
[36] B. R. A. Nijboer and L. Van Hove, Phys. Rev. **85**, 777 (1952).
[37] E. Krotscheck, M. D. Miller, and J. Wojdylo, Phys. Rev. B **60**, 13028 (1999).
[38] A. Sarsa, K. E. Schmidt, and W. R. Magro, J. Chem. Phys. **113**, 1366 (2000).
[39] D. E. Galli and L. Reatto, Mol. Phys. **101**, 1697 (2003).
[40] M. Rossi, M. Nava, L. Reatto, and D. E. Galli, J. Chem. Phys. **131**, 154108 (2009).
[41] E. Vitali, M. Rossi, L. Reatto, and D. E. Galli, Phys. Rev. B **82**, 174510 (2010).
[42] R. A. Cowley and A. D. B. Woods, Can. J. Phys. **49**, 177 (1971).
[43] K. Beauvois, C. E. Campbell, J. Dawidowski, B. Fåk, H. Godfrin, E. Krotscheck, H.-J. Lauter, T. Lichtenegger, J. Ollivier, and A. Sultan, Phys. Rev. B **94**, 024504 (2016).
[44] R. Ozeri, N. Katz, J. Steinhauer, and N. Davidson, Rev. Mod. Phys. **77**, 187 (2005).
[45] L.-C. Ha, L. W. Clark, C. V. Parker, B. M. Anderson, and C. Chin, Phys. Rev. Lett. **114**, 055301 (2015).
[46] R. Landig, F. Brennecke, R. Mottl, T. Donner, and T. Esslinger, Nat. Commun. **6**, 7046 (2015).
[47] S. Tomonaga, Prog. Theor. Phys. **5**, 544 (1950).
[48] J. M. Luttinger, J. Math. Phys. **4**, 1154 (1963).
[49] D. C. Mattis and E. H. Lieb, J. Math. Phys. **6**, 304 (1965).
[50] F. D. M. Haldane, Phys. Rev. Lett. **47**, 1840 (1981).
[51] F. D. M. Haldane, Phys. Rev. Lett. **48**, 569 (1982).
[52] A. Imambekov and L. I. Glazman, Phys. Rev. Lett. **102**, 126405 (2009).
[53] H. Bethe, Eur. Phys. J. A **71**, 205 (1931).
[54] G. E. Astrakharchik, J. Boronat, J. Casulleras, and S. Giorgini, Phys. Rev. Lett. **95**, 190407 (2005).
[55] M. T. Batchelor, M. Bortz, X. W. Guan, and N. Oelkers, J. Stat. Mech. (2005) L10001.
[56] E. Tempfli, S. Zöllner, and P. Schmelcher, New J. Phys. **10**, 103021 (2008).
[57] M. Panfil, J. De Nardis, and J.-S. Caux, Phys. Rev. Lett. **110**, 125302 (2013).
[58] A. H. Castro Neto, H. Q. Lin, Y.-H. Chen, and J. M. P. Carmelo, Phys. Rev. B **50**, 14032 (1994).
[59] A. Y. Cherny, J. S. Caux, and J. Brand, Front. Phys. **7**, 54 (2012).
[60] S. S. Shamailov and J. Brand, New J. Phys. **18**, 75004 (2016).
[61] J. S. Caux and P. Calabrese, Phys. Rev. A **74**, 031605 (2006).
[62] F. Meinert, M. Panfil, M. J. Mark, K. Lauber, J.-S. Caux, and H.-C. Nägerl, Phys. Rev. Lett. **115**, 085301 (2015).
[63] S. De Palo, E. Orignac, R. Citro, and M. L. Chiofalo, Phys. Rev. B **77**, 212101 (2008).
[64] M. Nava, D. E. Galli, S. Moroni, and E. Vitali, Phys. Rev. B **87**, 144506 (2013).
[65] F. Arrigoni, E. Vitali, D. E. Galli, and L. Reatto, Low Temp. Phys. **39**, 793 (2013).
[66] R. Rota, F. Tramonto, D. E. Galli, and S. Giorgini, Phys. Rev. B **88**, 214505 (2013).
[67] M. Holzmann, D. M. Ceperley, C. Pierleoni, and K. Esler, Phys. Rev. E **68**, 046707 (2003).
[68] M. H. Kalos and P. A. Whitlock, *Monte Carlo Methods*, 2nd ed. (Wiley, Hoboken, NJ, 1986).
[69] J. Toulouse and C. J. Umrigar, J. Chem. Phys. **126**, 084102 (2007).
[70] M. Motta, G. Bertaina, D. E. Galli, and E. Vitali, Comput. Phys. Commun. **190**, 62 (2015).

[71] N. Metropolis, A. W. Rosenbluth, M. N. Rosenbluth, A. H. Teller, and E. Teller, J. Chem. Phys. **21**, 1087 (1953).
[72] D. Ceperley, Rev. Mod. Phys. **67**, 279 (1995).
[73] J. Cao and B. J. Berne, J. Chem. Phys. **97**, 2382 (1992).
[74] F. De Soto and M. C. Gordillo, Phys. Rev. A **85**, 013607 (2012).
[75] A. Tarantola, Nat. Phys. **2**, 492 (2006).
[76] R. N. Silver, J. E. Gubernatis, D. S. Sivia, and M. Jarrell, Phys. Rev. Lett. **65**, 496 (1990).
[77] M. Jarrell and J. E. Gubernatis, Phys. Rep. **269**, 133 (1996).
[78] M. Boninsegni and D. M. Ceperley, J. Low Temp. Phys. **104**, 339 (1996).
[79] A. Roggero, F. Pederiva, and G. Orlandini, Phys. Rev. B **88**, 094302 (2013).
[80] A. S. Mishchenko, N. V. Prokofev, A. Sakamoto, and B. V. Svistunov, Phys. Rev. B **62**, 6317 (2000).
[81] M. Rossi, E. Vitali, L. Reatto, and D. E. Galli, Phys. Rev. B **85**, 014525 (2012).
[82] M. Nava, D. E. Galli, M. W. Cole, and L. Reatto, J. Low Temp. Phys. **171**, 699 (2013).
[83] S. Molinelli, D. E. Galli, L. Reatto, and M. Motta, J. Low Temp. Phys. **185**, 39 (2016).
[84] S. Saccani, S. Moroni, E. Vitali, and M. Boninsegni, Mol. Phys. **109**, 2807 (2011).
[85] S. Saccani, S. Moroni, and M. Boninsegni, Phys. Rev. Lett. **108**, 175301 (2012).
[86] E. Vitali, H. Shi, M. Qin, and S. Zhang, Phys. Rev. B **94**, 085140 (2016).
[87] M. Teruzzi, D. E. Galli, and G. Bertaina, arXiv:1607.05308.
[88] G. E. Astrakharchik and J. Boronat, Phys. Rev. B **90**, 235439 (2014).
[89] R. G. Pereira, K. Penc, S. R. White, P. D. Sacramento, and J. M. P. Carmelo, Phys. Rev. B **85**, 165132 (2012).
[90] G. Roux, A. Minguzzi, and T. Roscilde, New J. Phys. **15**, 055003 (2013).
[91] R. Citro, E. Orignac, S. De Palo, and M. L. Chiofalo, Phys. Rev. A **75**, 051602 (2007).
[92] G. E. Astrakharchik, D. M. Gangardt, Y. E. Lozovik, and I. A. Sorokin, Phys. Rev. E **74**, 021105 (2006).
[93] D. Petrosyan, M. Höning, and M. Fleischhauer, Phys. Rev. A **87**, 053414 (2013).